RSC Advances

PAPER

View Article Online
View Journal | View Issue

Check for updates

Cite this: *RSC Adv.*, 2025, **15**, 20111

Design of a magnetic Fenton-like catalyst by decorating diamond-shaped MIL-88A with *Chenopodium*-derived biochar for nitrophenol degradation: optimization and mechanistic insights†

Abdelazeem S. Eltaweil, *[a] Mohammed Salah Ayoup,[b] Jawaher Y. Al Nawah *[b] and Eman M. Abd El-Monaem[c]

Received 12th April 2025
Accepted 19th May 2025

DOI: 10.1039/d5ra02562a

rsc.li/rsc-advances

An effective Fenton-like Fe_3O_4/MIL-88A/BC catalyst was fabricated by combining magnetite nanoparticles (Fe_3O_4) with diamond-shaped MIL-88A and *Chenopodium*-derived biochar for the degradation of 2-NP. The elemental composition, morphology, functional groups, surface net charge, and crystallographic phase of the Fe_3O_4/MIL-88A/BC catalyst were examined using various characterization techniques, including XPS, SEM, FTIR, ZP, and XRD. Optimization experiments were conducted to determine the optimal Fenton-like degradation conditions for 2-NP using H_2O_2/Fe_3O_4/MIL-88A/BC. Laboratory experiments showed that the 2-NP degradation efficiency by H_2O_2/Fe_3O_4/MIL-88A/BC reached 91.04% within 120 min at pH = 5, Fe_3O_4/MIL-88A/BC = 10 mg, and H_2O_2 concentration = 500 mg L^{-1}. Kinetic studies indicated that the Fenton-like degradation of 2-NP followed a second-order model, while H_2O_2 decomposition was best described by a first-order model. Quenching tests indicated that the Fenton-like reaction of 2-NP proceeded *via* a radical mechanism and confirmed that the $^{\bullet}OH$ radicals are the controlling reactive O-species. The degradation mechanism of 2-NP was proposed based on the XPS spectra of the neat and used Fe_3O_4/MIL-88A/BC catalysts. The intermediates obtained from the Fenton-like degradation of 2-NP by the Fe_3O_4/MIL-88A/BC catalyst were predicted from the GC-MS spectrum.

1. Introduction

Recently, the world has delved deeply into the issue of water pollution, which threatens the survival of human beings and the entire planet. Scientists and environmental experts are challenged by this dilemma because most water contaminants are cogs in the wheel of vital industries. For instance, 2-NP is widely used in numerous industries, including fungicide, petrochemical, pigment, explosive, pharmaceutical, insecticide, chemical intermediate, and herbicide industries. The total annual production of 2-NP ranges from 10 to 15 million pounds.[1] Nonetheless, the leakage of even a relatively low concentration of 2-NP into water bodies could lead to harmful effects on human health, such as blurred vision, liver and kidney damage, drowsiness, mouth irritation, and cyanosis.[2] In addition, 2-NP has a disruptive impact on the environment, with its nitro-containing group contributing to its stability in water and soil.[3] Therefore, there is an essential need to investigate effective measures for controlling the presence of 2-NP in water bodies. Techniques such as adsorption, membrane filtration, electrolysis, coagulation, and Fenton degradation have progressed as promising approaches to tackle such hazardous compounds.[4,5]

The non-toxicity, plentiful iron sources, absence of secondary contaminant formation, and use of green oxidants make Fenton degradation a felicitous strategy to outdo 2-NP from wastewater.[6] Fenton reaction is one of the most efficacious hydroxyl radical-based advanced oxidation processes and has exhibited preeminent performance in degrading the notorious 2-NP. Generally, Fenton degradation of such persistent nitro-aromatic compounds proceeds *via* the formation of hydroxyl radicals ($^{\bullet}OH$) by the activation of hydrogen peroxide (H_2O_2) using iron-based catalysts.[7,8] However, iron-based catalysts still require further development to enhance the production of $^{\bullet}OH$ radicals and accelerate the Fe^{2+}/Fe^{3+} cycle.

Metal–organic frameworks (MOFs) are considered a recent breakthrough in material science revolution. The discernible

[a]*Chemistry Department, Faculty of Science, Alexandria University, Alexandria, Egypt. E-mail: abdelazeemeltaweil@alexu.edu.eg*

[b]*Department of Chemistry, College of Science, King Faisal University, Al-Ahsa 31982, Saudi Arabia. E-mail: jalnawah@kfu.edu.sa; mayoup@kfu.edu.sa*

[c]*Advanced Technology Innovation, Borg El-Arab, Alexandria, Egypt. E-mail: emanabdelmonaem5925@yahoo.com*

† Electronic supplementary information (ESI) available. See DOI: https://doi.org/10.1039/d5ra02562a

Open Access Article. Published on 13 June 2025. Downloaded on 3/31/2026 11:27:39 AM. This article is licensed under a Creative Commons Attribution-NonCommercial 3.0 Unported Licence.

Open Access Article. Published on 13 June 2025. Downloaded on 3/31/2026 11:27:39 AM. This article is licensed under a Creative Commons Attribution-NonCommercial 3.0 Unported Licence.

characteristics of MOFs, such as excellent thermal and mechanical properties, high surface area, and high porosity, render them appropriate for numerous applications, including drug delivery, sensors, gas separation, wastewater purification, and solar cells.[9,10] For wastewater purification, MOFs have demonstrated outstanding results in removing persistent pollutants *via* many remediation strategies. In particular, Fenton degradation is due to the individual chemical structures of the ligands, which contain unsaturated coordination species and abundant oxygen functional groups.[11] Iron-based MOFs, including MIL-101, MIL-88A, MIL-100, MIL-88B, and MIL-53, have demonstrated remarkable performance in degrading diverse contaminants by the Fenton degradation process. In particular, MIL-88A has gained exceptional interest as a remarkable Fenton catalyst owing to its high recyclability, efficient catalytic activity, and chemical stability.[12]

Biochar (BC) is a dust-carbon-rich substance derived from biowaste *via* thermal decomposition under pyrolysis temperatures in the range of 300–900 °C.[13,14] Interestingly, the conversion of biowaste, like agricultural waste, to BC could provide a better solution for removing this waste instead of burning it. Reported studies have demonstrated the hazardous impact of burning agricultural waste on human health, especially the respiratory system.[15] Thanks to the remarkable properties of BC, such as good mechanical strength, porous structure, high surface area, and possession of oxygenated groups, it makes it a superb catalyst for degrading pollutants by Fenton/Fenton-like reactions.[16] In addition, environmentally persistent free radicals (EPFRs)-containing BC can activate H_2O_2 to generate $^{\bullet}OH$ radicals during Fenton/Fenton-like reactions.[17]

Magnetite (Fe_3O_4) is a bright iron-based nanocatalyst that has demonstrated remarkable performance in Fenton degradation reactions of many harmful pollutants.[18] This auspicious catalytic performance of Fe_3O_4 stems from its Fe^{2+} ions, which activate H_2O_2 *via* the Haber–Weiss reaction and produce $^{\bullet}OH$ radicals.[19] Fe_3O_4 possesses an excellent ferromagnetic character, resulting in easy separation features that prevent mass loss during regeneration and save time during the separation step.[20] Additionally, Fe_3O_4 is a non-toxic substance with a wide surface area, good chemical stability, intrinsic peroxidase, and propitious recyclability.[21,22] Notably, the octahedral site in the Fe_3O_4 matrix allows it to accommodate Fe^{2+} and Fe^{3+}; therefore, the Fe^{2+} moieties can be oxidized reversibly by transferring electrons between Fe^{2+} and Fe^{3+}.[23,24]

The MIL-88A and/or BC-based heterogeneous catalysts exhibit eminent catalytic activity in Fenton degradation reactions of various organic contaminants. For instance, Ren *et al.* fabricated ZnO-decorated MIL-88A rods to degrade methylene blue, clarifying that the degradation percentage attained 96.15% after a reaction time of 40 min.[25] Abd El-Monaem *et al.* developed rod-shaped MIL-88A with $SnFe_2O_4$ and supported them on MXene sheets for degrading the anionic Congo red dye, achieving a promising degradation percentage of 100% after 60 min. In addition, the synergistic effect of the CR adsorption and the Fenton-like process was monitored, where the adsorption percentage of CR was 47.25%.[26] Liao and his coworkers compared the catalytic activity of rod, diamond, and spindle-shaped MIL-88A toward the Fenton degradation of phenol. The experimental findings demonstrated that the catalytic degradation efficiency of the rod-like MIL-88A toward phenol was higher than that of the other forms, where it fulfilled 100% after 15 min.[27] Moreover, Sang *et al.* study involved investigating the Fenton-like degradation of ciprofloxacin by natural pyrite/rice straw-derived biochar, revealing that the degradation percentage achieved 96.8% after 20 minutes.[28] Park and his coauthors fabricated Fe-impregnated sugarcane biochar for degrading Orange G throughout a Fenton-like reaction. The degradation percentage of Orange G reached 99.70% after 120 minutes using 0.5 g L^{-1} of the Fe-impregnated biochar at pH = 5.5.[29]

In light of previous studies, diamond-shaped MIL-88A and BC were not used to degrade o-NP by the Fenton-like reaction. Meanwhile, MIL-88A and BC exhibit high dispersity, which hinders their separation from the catalytic media after Fenton reactions. To overcome the high dispersity of MIL-88A and BC, they can be incorporated into polymeric materials and shaped into beads, hydrogels, or membranes. However, the degradation efficacy may decline because of the lower catalytic activity of the polymers. On the other hand, adding a magnetic substance to MIL-88A and BC results in a magnetic catalyst that can be separated perfectly from the catalytic media by an external magnet. Magnetic substances contain transition metals that exhibit remarkable activity toward degrading organic pollutants *via* Fenton/Fenton-like reactions.

Accordingly, our investigation aimed to take the merits of MIL-88A, Fe_3O_4, and BC to fabricate a Fenton-like catalyst with eminent catalytic activity, excellent chemical stability, and outstanding recyclability. Consequently, an Fe_3O_4/MIL-88A/BC composite was prepared, and its chemical and physical properties were studied using varied characterization tools, including XPS, FTIR, VSM, ZP measurements, SEM, and XRD. The optimum Fenton-like parameters for degrading 2-NP by Fe_3O_4/MIL-88A/BC were investigated after a series of degradation reactions at different pH values, catalyst doses, 2-NP and H_2O_2 concentrations, and temperatures. The kinetic models were applied to the experimental results obtained by degrading 2-NP and H_2O_2 over time. The chemical stability of the Fenton-like Fe_3O_4/MIL-88A/BC catalyst was confirmed by cycling tests and metal leaching studies after each recycling run. The Fenton-like degradation mechanism of o-NP by H_2O_2 activation using the Fe_3O_4/MIL-88A/BC catalyst was proposed based on the quenching test results and XPS spectra of fresh and used Fe_3O_4/MIL-88A/BC. The intermediates yielded from 2-NP degradation by Fe_3O_4/MIL-88A/BC were determined by GC-MS.

2. Materials and methods

2.1. Materials

The chemicals used in the preparation stage of the Fe_3O_4/MIL-88A/BC catalyst were Ferric chloride hexahydrate ($FeCl_3 \cdot 6H_2O$) and fumaric acid (FA), which were purchased from Aladdin Industrial Corporation (China). Ferrous chloride tetrahydrate was obtained from Sigma-Aldrich (USA). Ammonium solution (NH_4OH) and 2-NP were obtained from Sinopharm Chemical

© 2025 The Author(s). Published by the Royal Society of Chemistry

Open Access Article. Published on 13 June 2025. Downloaded on 3/31/2026 11:27:39 AM. This article is licensed under a Creative Commons Attribution-NonCommercial 3.0 Unported Licence.

Reagent (China). *N*,*N* dimethyl formamide (DMF) and ethanol (C_2H_5OH) were obtained from Shanghai Chemical Reagent Co., Ltd (China).

2.2. Preparation of Fe_3O_4/MIL-88A/BC catalyst

2.2.1. Preparation of MIL-88A. MIL-88A was fabricated using a solvothermal approach; in a beaker containing 50 mL DMF, 1.4 g of $FeCl_3 \cdot 6H_2O$ was added under stirring until complete dissolution of the iron salt. Then, 0.52 g of FA was dipped into a bright orange solution containing Fe^{3+} ions while continuously stirring for 1 h. The obtained metal/ligand solution was poured into an autoclave and heated at 120 °C for one day. The formed MIL-88A particles were collected, washed with DMF and C_2H_5OH, and dried at 50 °C for 16 h in an oven.[30]

2.2.2. Preparation of Fe_3O_4. Magnetic Fe_3O_4 was fabricated using the precipitation method under a nitrogen atmosphere. A solution of Fe^{3+}/Fe^{2+} ions was prepared by dissolving $FeCl_3 \cdot 6H_2O$ and $FeCl_2 \cdot 4H_2O$ in 200 mL of distilled water. Drops of NH_4OH were added slowly over the Fe^{3+}/Fe^{2+} solution until the pH reached 10, and then the chocolate brown particles were kept at 80 °C. After 90 min, Fe_3O_4 nanoparticles were collected using a magnet, washed with distilled water and ethanol, and dried at 65 °C for 10 h.[31]

2.2.3. Preparation of biochar. *Chenopodium* plants were collected from agricultural land in El-Behara, Egypt. *Chenopodium* was thoroughly cleaned with tap water, followed by distilled water. The clean plant was kept in an oven at 70 °C until complete drying and then cut into small pieces (~1 cm). Finally, dried *Chenopodium* was pyrolyzed at 400 °C for 4 h under anoxic conditions. The obtained black powder of BC was ground using a mortar and pestle and stored in a glass tube.

2.2.4. Preparation of Fe_3O_4/MIL-88A/BC composite. The Fe_3O_4/MIL-88A/BC catalyst was prepared using a post-synthetic approach, as shown in Fig. 1. In a beaker containing 20 mL of distilled water, 100 mg of MIL-88A was added under sonication for 30 min. Then, 20 mg of Fe_3O_4 and amounts of BC (5–20 wt%) were mixed into the MIL-88A suspension *via* continual sonication for 2 h. The Fe_3O_4/MIL-88A/BC composites were dried at 50 °C for 6 h. After fabricating the Fe_3O_4, MIL-88A, BC, and Fe_3O_4/MIL-88A/BC composites, the physical and chemical characteristics of these samples were inspected using various characterization tools, as elucidated in Text S1.†

2.3. Fenton-like degradation experiment

The Fenton-like reaction of 2-NP by activating H_2O_2 using an Fe_3O_4/MIL-88A/BC catalyst was studied as follows: (i) a comparison test between Fe_3O_4, MIL-88A, BC, and Fe_3O_4/MIL-88A/BC composites for evincing the synergistic effect between the composite's components and selecting the optimal BC proportion. (ii) Proceeding with the Fenton-like degradation of 2-NP at a pH range of 3–11 to pick out the optimum pH of the catalytic medium. (iii) Determine the economical dose of Fe_3O_4/MIL-88A/BC by proceeding with Fenton-like degradation of 2-NP using varied doses of the catalyst (5–20 mg). (iv) Studying the effect of oxidant concentration on the degradation aptitude of 2-NP at H_2O_2 concentrations ranging from 100 to 1000 mg L^{-1}. (v) Identifying the effect of the temperature of the Fe_3O_4/MIL-88A/BC-H_2O_2 catalytic system on the degradation efficacy of 2-NP. (vi) Investigating the influence of the 2-NP concentration (50–300 mg L^{-1}) on the degradation efficiency at the constant weight of Fe_3O_4/MIL-88A/BC. The undegraded 2-NP concentration was determined using a spectrophotometer at a maximum wavelength of 344 nm, and the degradation efficiency of 2-NP was estimated using eqn (1).

$$\text{Degradation efficiency, DE} = \frac{C_0 - C_t}{C_0} \times 100 \quad (1)$$

where C_0 is the initial 2-NP concentration, and C_t is the undegraded concentration of 2-NP after the Fenton-like degradation process.

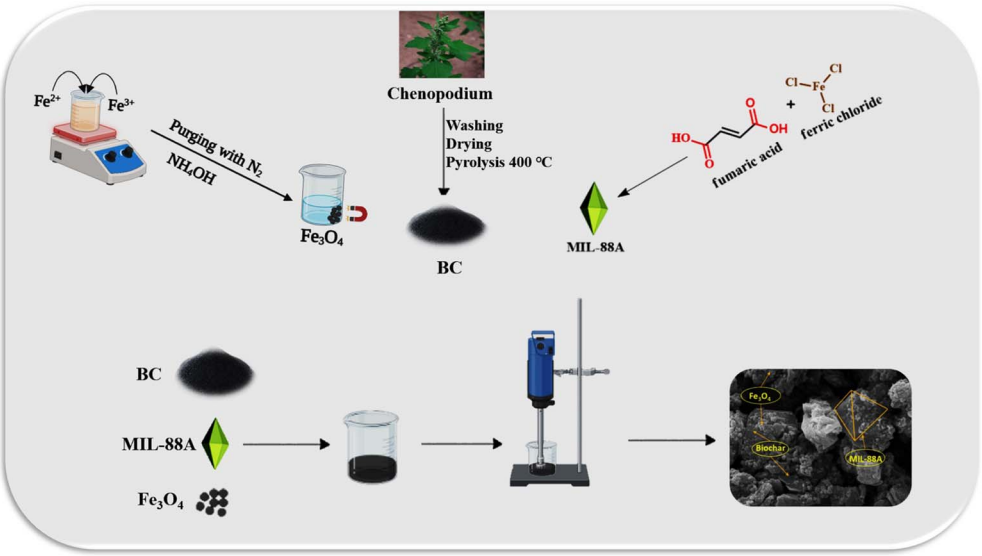

Fig. 1 Schematic representation of the fabrication process of the Fe_3O_4/MIL-88A/BC catalyst.

Open Access Article. Published on 13 June 2025. Downloaded on 3/31/2026 11:27:39 AM. This article is licensed under a Creative Commons Attribution-NonCommercial 3.0 Unported Licence.

2.4. Cycling test

The regeneration potential of the Fe_3O_4/MIL-88A/BC catalyst was assessed by performing the cycling test for five cycles. After the Fenton-like degradation of 2-NP was completed, the Fe_3O_4/MIL-88A/BC catalyst was collected using a magnet, washed with an aqueous solution of NaOH (1 M) and distilled water, and dried at 50 °C in an oven. Subsequently, the regenerated Fe_3O_4/MIL-88A/BC catalyst was tested in the next Fenton-like degradation cycle of 2-NP.

2.5. Extraction of the intermediate compounds

The intermediate compounds from degrading 2-NP by Fe_3O_4/MIL-88A/BC were extracted from the Fenton-like catalytic medium by a liquid–liquid extraction procedure as follows: adding 20 mL of the 2-NP solution after the Fenton-like degradation reaction and 20 mL of $C_4H_8O_2$ in a separatory funnel. After extracting the organic compounds, they were dried with Na_2SO_4 using rotary evaporation. Next, the extracted sample was dissolved in MeOH and injected into the GC-MS (PE-5MS column; 0.18 mm film thickness, 0.18 mm diameter, and 20 m length) at 80 °C with the temperature increasing by 10 °C min^{-1} until reaching 280 °C.[32]

3. Results and discussion

3.1. Studying the Fe_3O_4/MIL-88A/BC characteristics

Based on the experimental results, the Fe_3O_4/MIL-88A/BC composite containing 10 wt% BC exhibited the highest catalytic activity toward o-NP. Therefore, a characterization analysis was conducted on the catalyst containing 10 wt% BC.

3.1.1. FTIR. The chemical compositions and functional groups of the MIL-88A, Fe_3O_4, BC, and Fe_3O_4/MIL-88A/BC composites were investigated by FTIR analysis, as shown in Fig. 2A. The spectrum of MIL-88A shows FTIR peaks at the wavenumbers of 981 and 1213 cm^{-1} related to C–C and C–H bonds of the trans diene of FA; in addition, the Fe–O peak manifests at the wavenumber of 554 cm^{-1}. The C=O peaks of the carboxylate groups of FA appeared at wavenumbers of 1551 cm^{-1} (asymmetric C=O) and 1398 cm^{-1} (symmetric C=O). The wide-broad band between 3354 and 3514 cm^{-1} is attributed to OH groups.[23–25] The FTIR spectrum of Fe_3O_4 demonstrated the chemical functional groups of Fe_3O_4, which revealed the accredited peaks to Fe–O–Fe at wavenumbers of 559 and 1402 cm^{-1}. In addition, the FTIR peaks of bending OH appeared at 1634 cm^{-1}, and vibrating OH appeared at

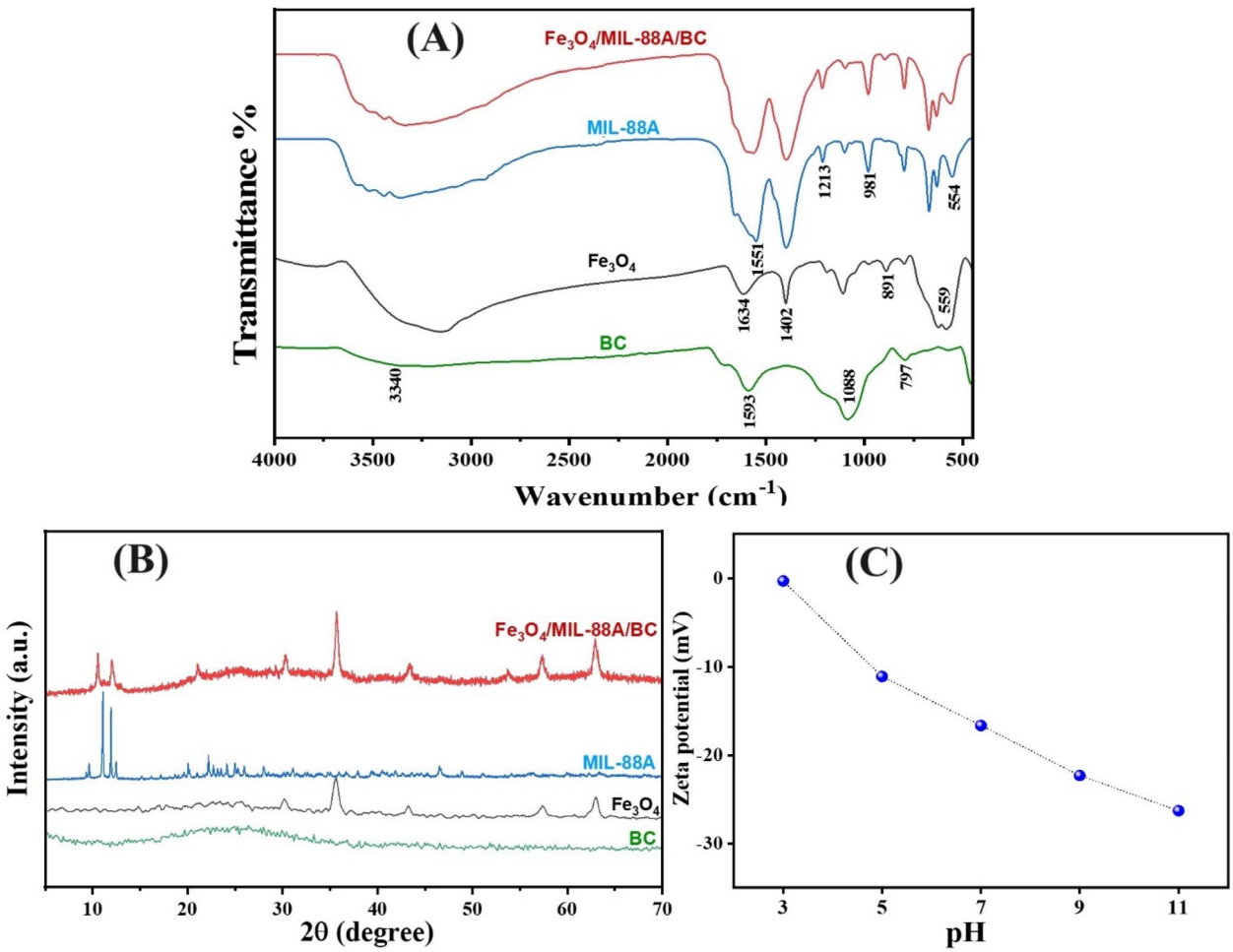

Fig. 2 (A) FTIR spectra, (B) XRD of MIL-88A, Fe_3O_4, BC, and Fe_3O_4/MIL-88A/BC composites, and (C) zeta potentials of the Fe_3O_4/MIL-88A/BC composites.

© 2025 The Author(s). Published by the Royal Society of Chemistry

Open Access Article. Published on 13 June 2025. Downloaded on 3/31/2026 11:27:39 AM. This article is licensed under a Creative Commons Attribution-NonCommercial 3.0 Unported Licence.

891 cm^{-1}.[26,27] The spectrum of BC shows FTIR peaks at 458 and 1088 cm^{-1}, which are assigned to Si–O and C–O, respectively. The C–H peak appeared at 797 cm^{-1}, and the peak at 1593 cm^{-1} corresponded to C=C.[28] The FTIR spectrum of the Fe_3O_4/MIL-88A/BC composite denoted the well-blending of MIL-88A, Fe_3O_4, and BC, where their distinguishing bands are obvious.

3.1.2. XRD. The crystallographic phases of the MIL-88A, Fe_3O_4, BC, and Fe_3O_4/MIL-88A/BC composites were determined from the XRD patterns (Fig. 2B). The crystalline pattern of MIL-88A shows distinct peaks at 2θ 9.54°, 11.12°, 11.90°, 20.27°, 22.02°, and 24.03° corresponding to the planes 011, 101, 002, 201, 103, and 202, respectively.[29] The pattern of Fe_3O_4 illustrates the XRD characteristic peaks at 2θ 30.23°, 35.79°, 43.20°, 57.09°, and 62.79°, which belong to the 220, 311, 400, 511, and 440 planes, respectively. The XRD profile of the *Chenopodium*-based BC showed a broad peak between 2θ 14.17° and 37.28°, indicating a typical amorphous structure of BC.[2] The pattern of the Fe_3O_4/MIL-88A/BC composite confirmed the combination of Fe_3O_4, MIL-88A, and BC, where the distinguishing peaks of MIL-88A and Fe_3O_4 appeared with a slight shift and decline in their intensity, with the existence of the amorphous peak of BC at the same peak area.

3.1.3. Zeta potential. The amount of charge carried on the surface of the Fe_3O_4/MIL-88A/BC catalyst was investigated by zeta potential measurements (Fig. 2C). The results implied the existence of high negative charges on the catalyst's surface that increased with increasing pH from 3 to 11, where the zeta potential augmented from −0.315 to −26.30 eV sequentially. This high negative charge on the Fe_3O_4/MIL-88A/BC surface is most likely due to the oxygen-containing functional groups (*viz.*, COOH and OH) that share electrons during Fenton-like degradation to activate H_2O_2 and yield $^{\bullet}OH$.

3.1.4. XPS. The elemental compositions of the Fe_3O_4/MIL-88A/BC composites were determined by XPS analysis. The wide XPS spectrum exhibited three characteristic peaks for C 1s, Fe 2p, and O 1s at 285.99, 712.04, and 531.84 eV, respectively. The atomic percentages of carbon, iron, and oxygen were 49.56%, 8.57%, and 41.88%, respectively. The high resolution of O 1s (Fig. 3A) clarified the corresponding peak to the carboxylate group of FA at 531.15 eV; in addition, the peaks of Fe–O–Fe and C–O appeared at 529.56 and 531.18 eV, respectively. The high-resolution spectrum of C 1 s (Fig. 3B) reveals the XPS peaks at 288.42 and 286.18 eV that are attributed to C=O and C–O, and the peak at 284.67 eV corresponds to C–H and C–C. The peaks located in the Fe 2P spectrum (Fig. 3C) at 710.35 and 712.47 eV

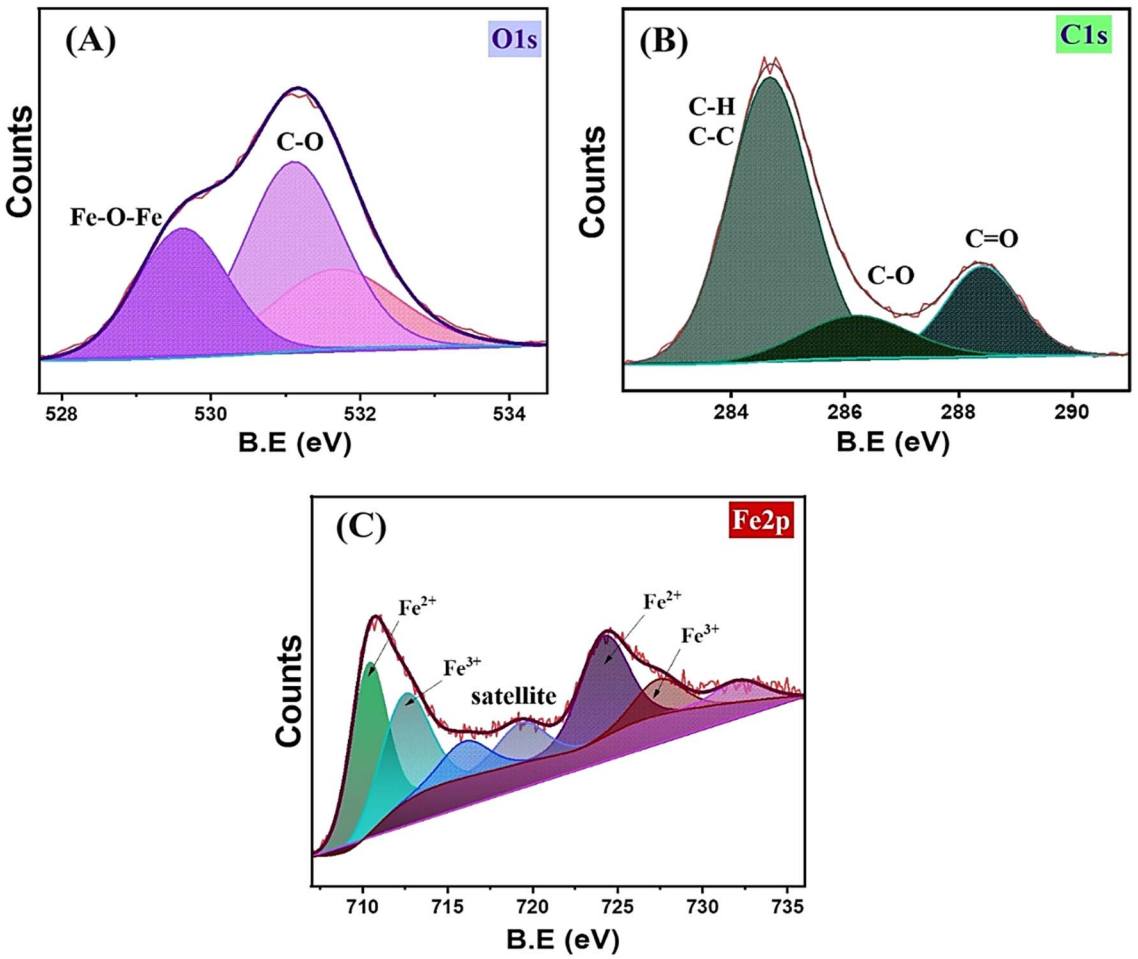

Fig. 3 XPS spectra of the Fe_3O_4/MIL-88A/BC composite: (A) O 1s, (B) C 1s, and (C) Fe 2p.

Open Access Article. Published on 13 June 2025. Downloaded on 3/31/2026 11:27:39 AM. This article is licensed under a Creative Commons Attribution-NonCommercial 3.0 Unported Licence.

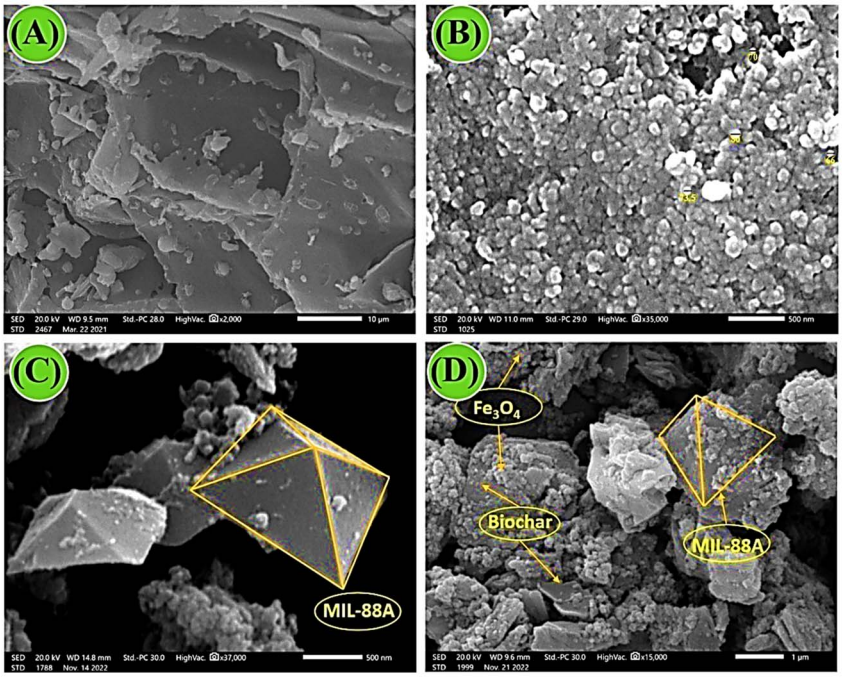

Fig. 4 SEM images of (A) BC, (B) Fe_3O_4, (C) MIL-88A, and (D) Fe_3O_4/MIL-88A/BC composite.

are assigned to Fe^{2+} and Fe^{3+} of $Fe2p_{3/2}$, respectively, and their satellite peaks exist at 716.01 and 719.36 eV. The XPS peaks of $Fe2p_{1/2}$ at 724.16 and 727.42 eV belong to Fe^{2+} and Fe^{3+}, respectively, whereas the satellite peak appeared at 732.16 eV.

3.1.5. SEM. The SEM images (Fig. 4A–D) show the outer morphologies of the MIL-88A, Fe_3O_4, BC, and Fe_3O_4/MIL-88A/BC composites. The SEM image shows that the morphology of the BC surface is quite rough with some burs. This specification of the BC surface enables it to be a supporter of MIL-88A and Fe_3O_4. The Fe_3O_4 morphology was manifested in the SEM images as quasi-spheroidal particles with nanoscale sizes. The SEM image shows the diamond-like morphology of MIL-88A, which is one of the most famous shapes of MIL-88A that is fabricated *via* a solvothermal approach using DMF as a solvent. The SEM of Fe_3O_4/MIL-88A/BC revealed clumps of Fe_3O_4 on the diamond-like particles of MIL-88A supported on the surface of BC.

3.2. Optimizing the Fenton-like degradation process of 2NP

3.2.1. Comparison test. A series of Fenton-like degradation experiments on 2-NP (Fig. 5A) were conducted using Fe_3O_4, MIL-88A, BC, and Fe_3O_4/MIL-88A/BC composites as catalysts under the same reaction conditions. Additionally, the Fenton-like reaction of 2-NP was conducted using H_2O_2 alone without the addition of a catalyst. An inferior DE of 2-NP was recorded in the presence of H_2O_2 only (9.46%), suggesting the importance of the catalyst for activating H_2O_2 and producing free radicals. The DE of 2-NP prepared using Fe_3O_4, MIL-88A, and BC was 46.05%, 63.75%, and 35.56%, respectively. Furthermore, the Fe_3O_4/MIL-88A/BC composites with varied proportions of BC exhibited degradation percentage of 2-NP by 58.51%, 64.05%, 80.25%, and 71.97% when the doped BC amounts were 5, 7, 10, and 20 wt%. The former results demonstrated a synergistic effect between iron-based catalysts (Fe_3O_4 and MIL-88A) and EPFR-containing BC, which work together to activate H_2O_2 and generate $^{\bullet}OH$ radicals.[17] Moreover, it was noticed that there was an increment in the DE of 2-NP when the doped proportion of BC was augmented from 5 to 10 wt%, whereas the over-increment in the doped BC amount in the catalyst decreased the DE of 2-NP. This finding may be due to the aggregation of the excess proportion of BC, which diminished the available surface area of the Fe_3O_4/MIL-88A/BC catalyst.[6] Thus, the Fe_3O_4/MIL-88A/BC catalyst, which contained 10 wt% BC, was used to perform the rest of the o-NP Fenton-like degradation experiments.

3.2.2. Influence of pH. Since the Fenton-like process is quite sensitive to the pH of the catalytic reaction media, the Fenton-like degradation of 2-NP was examined in the pH range of 3–11, as illustrated in Fig. 5B. The experimental results showed that the best pH for degrading 2-NP was at a low acidic medium and near alkaline medium (DE = 80.25% at pH 5). In addition, a significant decline in the DE of 2-NP was observed in the presence of a lower acidic and higher alkaline media. These findings may be ascribed to the higher redox potential of H_2O_2 in acidic medium ($E^0 = 2.7$ eV) than in alkaline medium ($E^0 = 1.8$ eV), so the $^{\bullet}OH$ radicals produced in a highly acidic medium are lower.[33] In addition, the abundant H^+ in a highly acidic medium retards $^{\bullet}OH$ degradation during the reaction of 2-NP molecules. Moreover, a significant decline in the DE of 2-NP reached its half value under highly basic conditions, where the high concentrations of hydroxyl radicals resulted in the formation of hydro-peroxy anions with potent affinity toward

© 2025 The Author(s). Published by the Royal Society of Chemistry

Open Access Article. Published on 13 June 2025. Downloaded on 3/31/2026 11:27:39 AM.
This article is licensed under a Creative Commons Attribution-NonCommercial 3.0 Unported Licence.

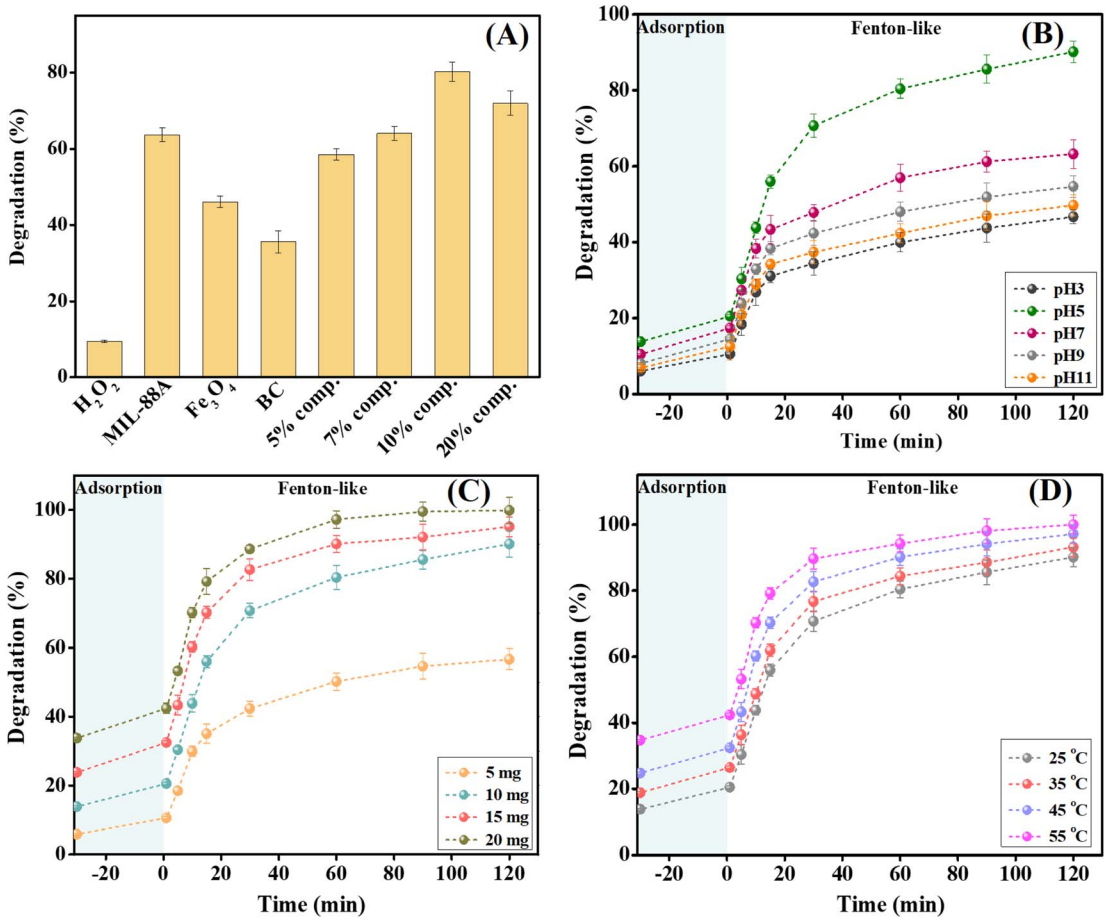

Fig. 5 (A) Comparison test (dose = 10 mg, temperature = 25 °C, [2-NP] = 50 mg L^{-1}, [H_2O_2] = 500 mg L^{-1}, and pH = 5); (B) effect of pH on the catalytic system (dose = 10 mg, [H_2O_2] = 500 mg L^{-1}, temperature = 25 °C, [2-NP] = 50 mg L^{-1}, and pH = 3–11); (C) effect of catalyst dose ([H_2O_2] = 500 mg L^{-1}, temperature = 25 °C, [2-NP] = 50 mg L^{-1}, pH = 5, and dose = 5–20 mg); and (D) effect of temperature on the Fenton-like degradation of 2-NP (temperature = 25–55 °C, [2-NP] = 50 mg L^{-1}, pH = 5, [H_2O_2] = 500 mg L^{-1}, and dose = 10 mg).

attaching metal species (eqn (2) and (3)). The auto-decomposition of H_2O_2 in highly basic media to oxygen and water decreases the generated $^{\bullet}OH$ and weakens the degradation aptitude of 2-NP, as elucidated in eqn (4). Notably, the higher adsorption percentage of 2-NP was 13.84% at pH = 5 and the p*K*a of 2-NP = 7.23, indicating that it is an anionic molecule in alkaline media.[34,35] Consequently, it was deduced that electrostatic interactions do not participate in 2-NP adsorption, and other adsorption pathways are the governing mechanisms, like pi–pi interaction, electron donor–acceptor interaction, and H-bonds.[36]

$$H_2O_2 + OH^- \rightarrow OOH^- + H_2O \quad (2)$$

$$M + OOH^- \rightarrow M\cdots{}^{\bullet}OOH \quad (3)$$

$$2H_2O_2 \rightarrow O_2 + 2H_2O \quad (4)$$

3.2.3. Influence of the Fe_3O_4/MIL-88A/BC dose. Fig. 5C shows the dosage influence of the Fenton-like Fe_3O_4/MIL-88A/BC catalyst on the degradation aptitude of 2-NP. The experimental results clarified a drastic enhancement in the DE of 2-NP from 50.77% to 99.27% by elevating the dose of Fe_3O_4/MIL-88A/BC from 5 to 20 mg. This improvement in the DE of 2-NP is most likely due to the production of greater concentrations of $^{\bullet}OH$ radicals by the higher catalyst dose, which could directly attack higher concentrations of 2-NP molecules.[37] Moreover, increasing the Fe_3O_4/MIL-88A/BC catalyst dosage enhanced the adsorption percentage of 2-NP from 5.88% to 33.76% due to the plentiful adsorption groups provided by the high doses of Fe_3O_4/MIL-88A/BC.

3.2.4. Influence of the temperature. Fig. 5D shows the influence of the catalytic system temperature on the Fenton-like degradation of 2-NP by H_2O_2 activation using Fe_3O_4/MIL-88A/BC. It was observed that the DE of 2-NP increased from 80.25 to 90.63% when the temperature of the catalytic system was increased from 25 to 55 °C, subsequently. Such an increment in the 2-NP degradation percentage is due to increasing the interaction between H_2O_2 and the Fe_3O_4/MIL-88A/BC catalyst with increasing the temperature, which produces higher amounts of $^{\bullet}OH$ radicals.[38] Likewise, the adsorption percentage of 2-NP increased from 13.84% to 34.76% by raising the reaction temperature from 25 to 55 °C due to fastening the Brownian motion of 2-NP molecules, which increased the number of 2-NP molecules reaching the Fe_3O_4/MIL-88A/BC surface.

© 2025 The Author(s). Published by the Royal Society of Chemistry

Open Access Article. Published on 13 June 2025. Downloaded on 3/31/2026 11:27:39 AM. This article is licensed under a Creative Commons Attribution-NonCommercial 3.0 Unported Licence.

3.2.5. Influence of oxidant concentration. The impact of the oxidant concentration on the efficiency of 2-NP degradation was inspected at H_2O_2 concentrations ranging from 100 to 1000 mg L^{-1}, as shown in Fig. 6A. The DE of 2-NP increased from 70.70% to 80.25% when the H_2O_2 concentration was increased from 100 to 500 mg L^{-1} because of the increase in the production of $^{\bullet}OH$ radicals due to the abundant concentration of H_2O_2. Nevertheless, the excess concentration of H_2O_2 (over 500 mg L^{-1}) diminished the DE of 2-NP to 72.62% because higher concentrations of H_2O_2 could attack the presented $^{\bullet}OH$ radicals in the catalytic medium and generate $^{\bullet}OOH$ species, as elucidated in eqn (5) and (6).

$$H_2O_2 + {}^{\bullet}OH \rightarrow HOO^{\bullet} + H_2O \quad (5)$$

$$HOO^{\bullet} + {}^{\bullet}OH \rightarrow H_2O + O_2 \quad (6)$$

3.2.6. Decomposition of H_2O_2. The decomposition percentage of H_2O_2 with time controls the generated amount of $^{\bullet}OH$ radicals and the catalytic reaction time. Consequently, the decomposition percentage of the optimal H_2O_2 concentration (500 mg L^{-1}) by Fe_3O_4/MIL-88A/BC in the absence of 2-NP was examined, as shown in Fig. 6B. The results clarified that the decomposition percentage of H_2O_2 reached 98.78% after 120 minutes, implying the auspicious catalytic activity of Fe_3O_4/MIL-88A/BC and its high affinity toward activating H_2O_2.

3.2.7. Influence of the 2-NP concentrations. Fig. 6C demonstrates the Fenton-like activity of Fe_3O_4/MIL-88A/BC toward the degradation of 2-NP at different concentrations over 120 min. The results elucidated an improvement in the DE of 2-NP by increasing the degradation time up to 120 min, in which the 2-NP degradation percentage reached 91.04, 77.59, 66.97, and 58.99 when the initial 2-NP concentrations were 50, 100, 200, and 300 mg L^{-1}, respectively. A decline in the degradation percentage of 2-NP was noticed with increasing the initial concentrations of 2-NP, most likely due to the insufficient $^{\bullet}OH$ radicals to degrade these high concentrations of 2-NP. Similarly, the adsorption percentage of 2-NP declined from 13.84% to 10.25%, 7.28%, and 4.85% by augmenting the 2-NP concentrations because of the lower adsorption sites of Fe_3O_4/MIL-88A/BC for high 2-NP concentrations.[39]

3.3. Kinetics study

Regression analyses for the obtained results from the Fenton-like degradation reaction of 2-NP by the H_2O_2/Fe_3O_4/MIL-88A/

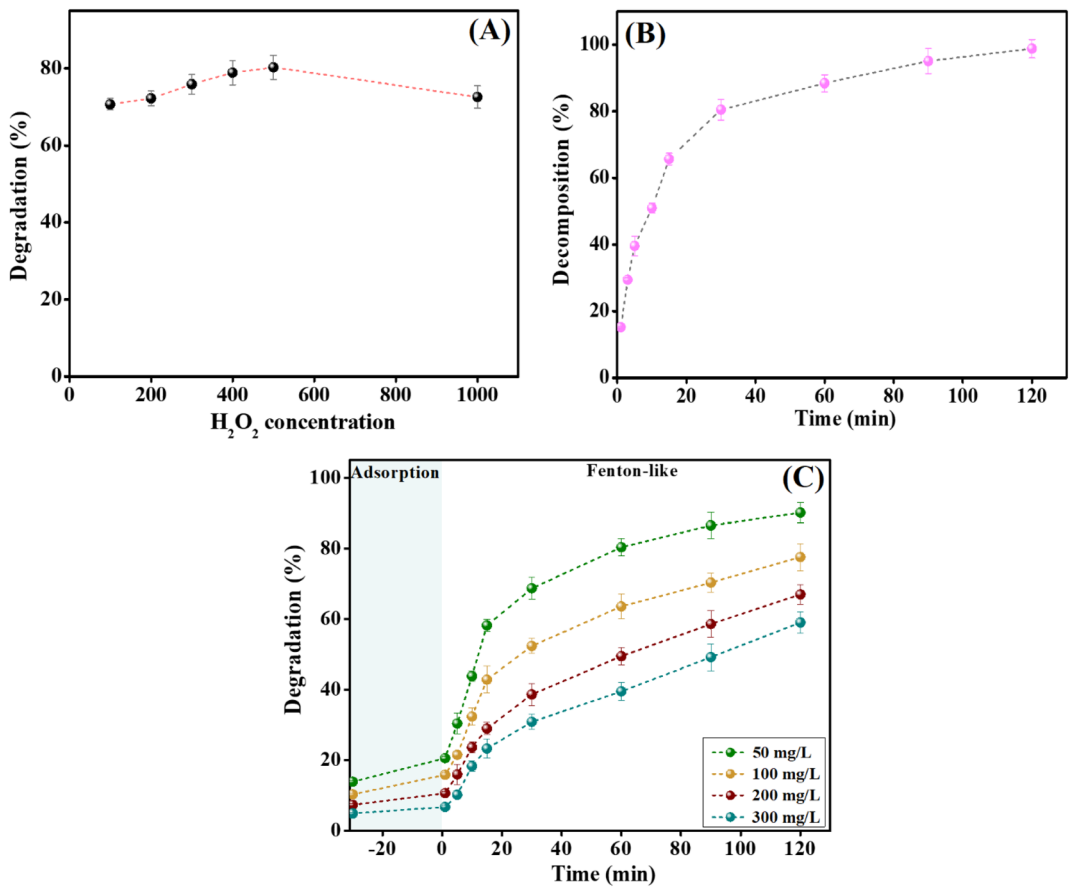

Fig. 6 (A) Effect of oxidant concentrations (pH = 5, [2-NP] = 50 mg L^{-1}, [H_2O_2] = 100–1000 mg L^{-1}, catalyst dose = 10 mg, and temperature = 25 °C), (B) decomposition of H_2O_2 ([2-NP] = 50 mg L^{-1}, pH = 5, [H_2O_2] = 500 mg L^{-1}, catalyst dose = 10 mg, and temperature = 25 °C); and (C) effect of 2-NP concentrations on the Fenton-like degradation efficiency ([2-NP] = 50–300 mg L^{-1}, pH = 5, [H_2O_2] = 500 mg L^{-1}, catalyst dose = 10 mg, and temperature = 25 °C).

© 2025 The Author(s). Published by the Royal Society of Chemistry

Open Access Article. Published on 13 June 2025. Downloaded on 3/31/2026 11:27:39 AM.
This article is licensed under a Creative Commons Attribution-NonCommercial 3.0 Unported Licence.

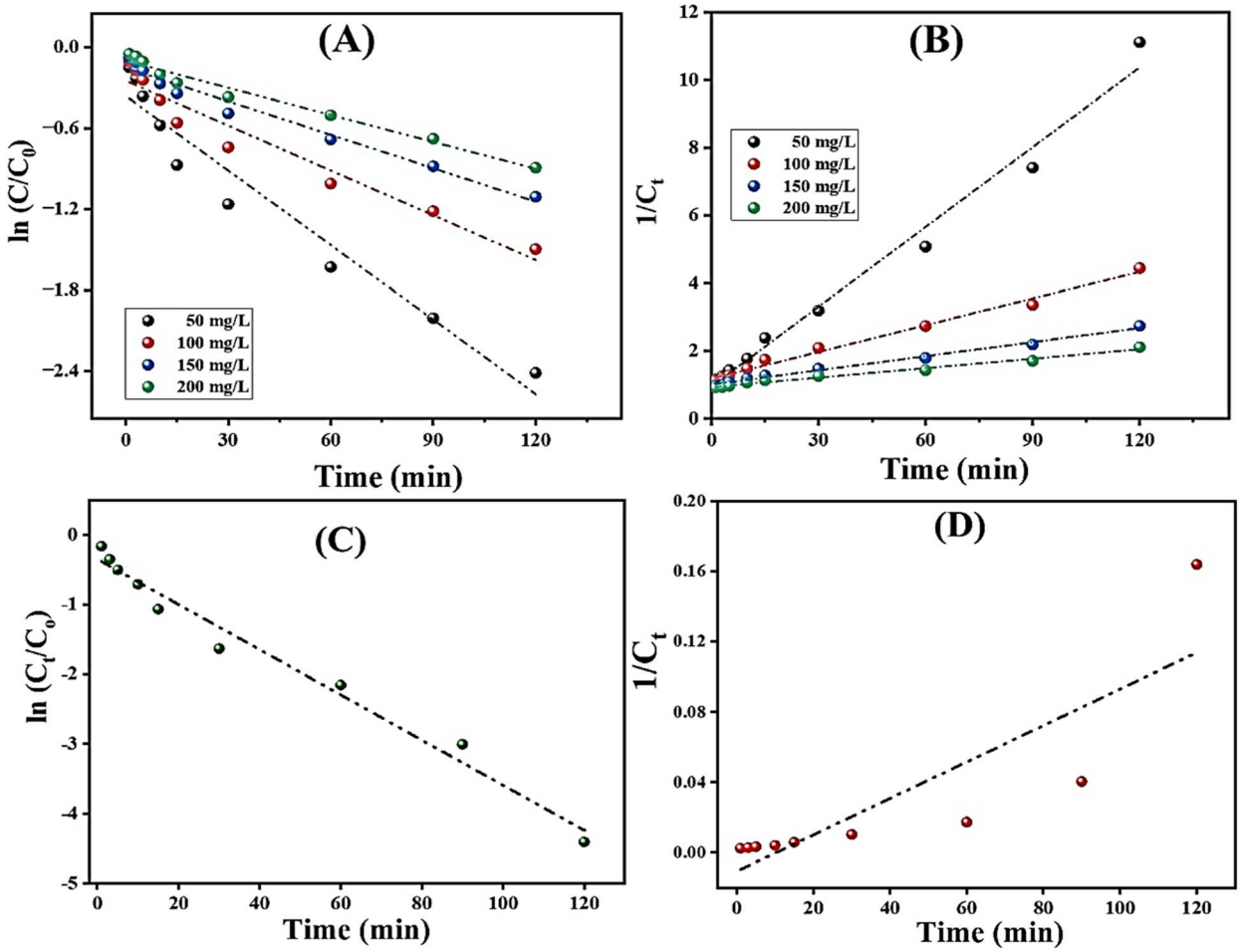

Fig. 7 Kinetic study of the Fenton-like degradation of 2-NP by the H_2O_2/Fe_3O_4/MIL-88A/BC system: (A) first-order and (B) second-order, and kinetic study of the H_2O_2 decomposition: (C) first-order and (D) second-order.

BC system were performed based on First-order and Second-order (eqn (7) and (8)).

$$\ln\frac{C_t}{C_0} = -k_1 t \quad (7)$$

$$\frac{1}{C_t} = \frac{1}{C_0} + k_2 t \quad (8)$$

C_t and C_0 are the 2-NP concentrations at a certain time and the initial reaction time, respectively. k_1 and k_2 are the rate constants of First-order and Second-order processes, respectively.

As illustrated in Fig. 7A, B and Table 1, the Fenton-like degradation reaction of 2-NP by the H_2O_2/Fe_3O_4/MIL-88A/BC system fits the Second-order more than the First-order, where the derived R^2 values from the Second-order are higher at varied 2-NP concentrations.[40] Notably, k_1 and k_2 are the slopes of the First-order plot ($\ln C_t/C_0$ *vs.* time) and Second-order plot ($1/C_t$ *vs.* time). The rate constants of the Fenton-like degradation of 2-NP based on the Second-order model were 0.0785, 0.0263, 0.0139, and 0.0093 mg L^{-1} min^{-1} when the initial 2-NP concentrations were 50, 100, 200, and 300 mg L^{-1}, respectively. The rate constant of the degradation reaction of 2-NP decreased as the initial 2-NP concentration increased, which may be due to the governing of some factors, including $^{\bullet}OH$ production and consumption; in addition, the competition between 2-NP and its degradation intermediates.[41,42] The kinetic study of H_2O_2 decomposition was conducted by analyzing the experimental data using first-order and second-order models (Fig. 7C and D). The derived kinetic parameters clarified the suitability of the first-order model for H_2O_2 decomposition by Fe_3O_4/MIL-88A/

Table 1 Derived parameter of the kinetic study of Fenton-like degradation of 2-NP

	Concentrations (mg L^{-1})			
Kinetic model	50	100	200	300
First order				
k_1	0.0185	0.0111	0.0083	0.0067
R^2	0.950	0.947	0.973	0.975
Second order				
k_2	0.0785	0.0263	0.0139	0.0093
R^2	0.985	0.990	0.992	0.985

© 2025 The Author(s). Published by the Royal Society of Chemistry

Open Access Article. Published on 13 June 2025. Downloaded on 3/31/2026 11:27:39 AM.
This article is licensed under a Creative Commons Attribution-NonCommercial 3.0 Unported Licence.

BC, where the R^2 values of the first-order and second-order models were 0.977 and 0.692, respectively. Furthermore, the decomposition rate constant was determined as 0.032 min^{-1} using first-order kinetics calculations.

3.4. Fenton-like degradation mechanism

3.4.1. Quenching test. To determine whether the controlling reactive O-species is ˙OH or superoxide ($O_2^{\cdot-}$), quenching tests were performed using chloroform and t-butanol for scavenging $O_2^{\cdot-}$ and ˙OH, respectively.[43] The scavenger test (Fig. 8A) implied that ˙OH is the dominant reactive O-species, where the Fenton-like degradation efficiency of 2-NP declined by 31.02% and 1.8% in the presence of *t*-butanol and chloroform, respectively. Such a finding denoted that the Fenton-like degradation mechanism of 2-NP by the H_2O_2/Fe_3O_4/MIL-88A/BC catalytic system follows a radical pathway, not surface oxygen vacancies.[44,45]

3.4.2. XPS analysis. Based on experimental observations, 2-NP degradation occurred *via* adsorption and a Fenton-like reaction. First, the corresponding peaks of nitrogen in the XPS survey of the Fe_3O_4/MIL-88A/BC catalyst evinced the adsorption reaction of 2-NP (Fig. 8B). This adsorption reaction between 2-NP and Fe_3O_4/MIL-88A/BC could proceed by the Pi–Pi interactions between the benzene rings in 2-NP and the catalyst. Electron donor–acceptor interactions may participate in the adsorption reaction of 2-NP by transferring electrons from the electron donor groups of Fe_3O_4/MIL-88A/BC (carboxyl and hydroxyl) to the electron acceptor nitro group of the 2-NP molecule. In addition, the hydroxyl group of 2-NP formed a coordination bond with the iron species in the Fe_3O_4/MIL-88A/BC catalyst. Moreover, H-bonds could be formed between the nitrogen and oxygen atoms of 2-NP and the hydrogen atoms of Fe_3O_4/MIL-88A/BC, whereas the oxygen atoms of the catalyst could create H-bonds with the hydrogen atoms of 2-NP molecules.

Second, the Fenton-like degradation reaction of 2-NP by Fe_3O_4/MIL-88A/BC was based on the XPS spectra that implied governing the Haber–Weiss mechanism in the degradation reaction as follows: The Fe 2p spectra (Fig. 8C) of the used and fresh Fe_3O_4/MIL-88A/BC catalysts showed a significant increment in the Fe^{3+}/Fe^{2+} ratio from 0.35 to 0.63, reflecting the consumption of Fe^{2+} in the H_2O_2 activation to produce ˙OH as represented in eqn (9). Furthermore, the XPS peaks of Fe^{2+} shifted from 710.35 and 724.16 eV to 710.30 and 723.85 eV; in addition, the peaks of Fe^{3+} also shifted from 712.24 and 727.24 eV to 713.05 and 727.03 eV. The continuous Fenton-like reaction of 2-NP requires a sustained and fast $Fe^{3+} \rightarrow Fe^{2+}$ redox cycle; thus, the electron-rich BC can supply the redox cycle with

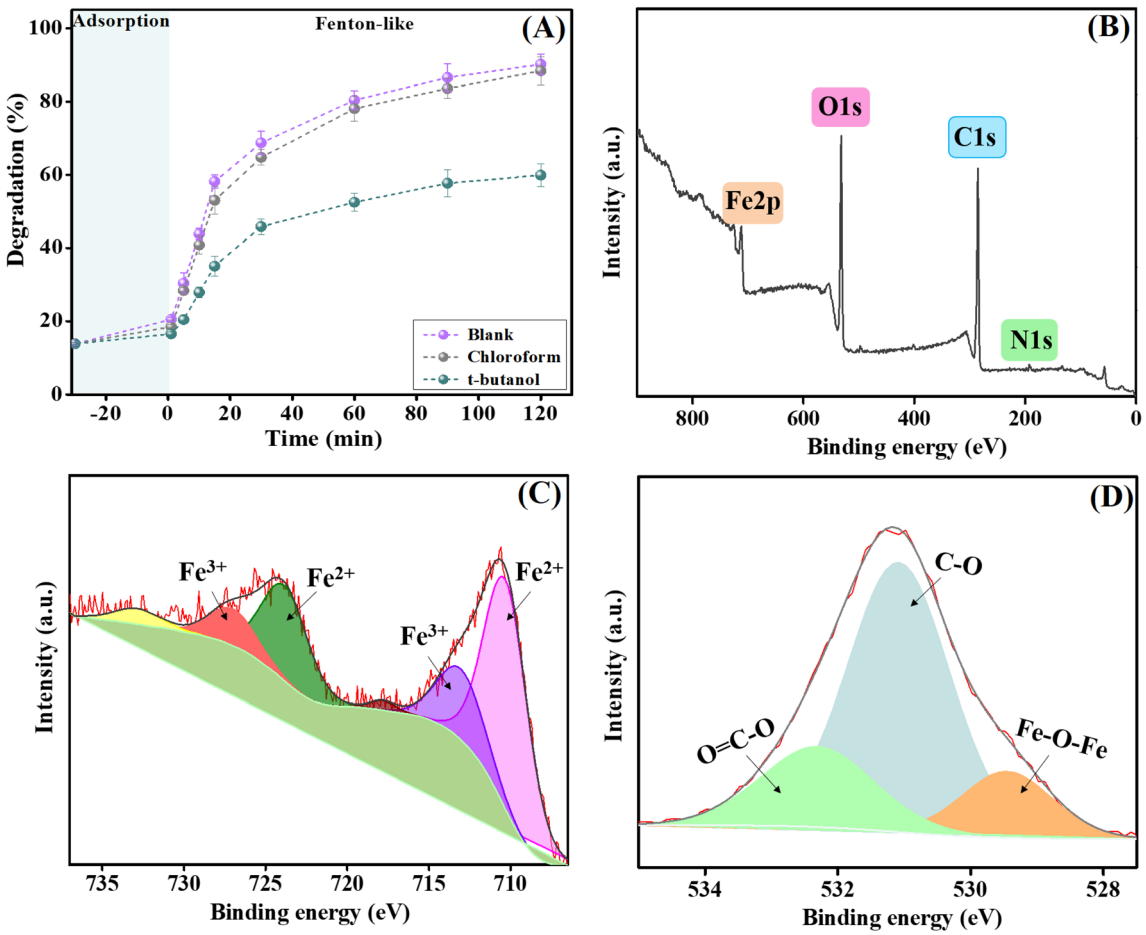

Fig. 8 (A) Quenching test of the Fe_3O_4/MIL-88A/BC, (B) XPS survey of the used Fe_3O_4/MIL-88A/BC catalyst, (C) high resolution of Fe 2p, and (D) high resolution of O 1s.

© 2025 The Author(s). Published by the Royal Society of Chemistry

Open Access Article. Published on 13 June 2025. Downloaded on 3/31/2026 11:27:39 AM. This article is licensed under a Creative Commons Attribution-NonCommercial 3.0 Unported Licence.

high amounts of electrons that facilitate the reduction of Fe^{3+} to Fe^{2+} (eqn (10)).

$$Fe^{2+} + H_2O_2 \rightarrow Fe^{3+} + {}^{\bullet}OH + {}^{-}OH \quad (9)$$

$$Fe^{3+} + e^{-} \rightarrow Fe^{2+} \quad (10)$$

Furthermore, oxygen-centered EPFRs activate H_2O_2, generating $^{\bullet}OH$ radicals (eqn (11)). The O 1s spectrum (Fig. 8D) of the Fe_3O_4/MIL-88A/BC exhibited a peak shifting of the C=O, C–O, and Fe–O–Fe from 531.15, 531.18, and 529.56 eV to 531.08, 532.31, and 529.45 eV, respectively. Furthermore, the intensity of C–O and Fe–O–Fe peaks decreased, whereas the peak intensity of C=O increased after the Fenton-like degradation of 2-NP. These observations implied the participation of C=O, C–O, and Fe–O–Fe in the Fenton-like reaction of 2-NP using the H_2O_2/Fe_3O_4/MIL-88A/BC catalytic system. Hence, we could conclude the significant role of BC that is not only responsible for half of the redox cycle ($Fe^{3+} \rightarrow Fe^{2+}$) but also contributes to H_2O_2 activation and $^{\bullet}OH$ radical production. Finally, the produced $^{\bullet}OH$, even by the Haber–Weiss mechanism or EPFRs-based BC, can attack o-NP molecules and degrade them to CO_2 and H_2O, as clarified in eqn (12).

$$EPFRs + H_2O_2 \rightarrow {}^{\bullet}OH + {}^{-}OH \quad (11)$$

$$2\text{-NP} + {}^{\bullet}OH \rightarrow \text{byproducts} \rightarrow CO_2 + H_2O \quad (12)$$

3.5. Degradation pathway

The suggested degradation pathway and the intermediates formed during the Fenton-like degradation of 2-NP onto the Fe_3O_4/MIL-88A/BC composite were analyzed using GC-MS (Fig. 9). The $^{\bullet}OH$ radicals attacked 2-NP *via* two distinct pathways. Fig. 10 illustrates the possible Fenton-like degradation pathway of 2-NP on the Fe_3O_4/MIL-88A/BC composite.

In the first pathway, the hydrogen atom of the phenyl ring at position 4 was substituted, leading to the formation of nitrohydroquinone, which appeared at a retention time (RT) of 11.81 min. Subsequently, the nitro group was replaced by OH, forming a hydroquinone radical that was converted into hydroquinone (RT = 23.87 min). Hydroquinone was further oxidized to *p*-benzoquinone (RT = 10.19 min), whose oxidative cleavage ultimately yielded CO_2 and water. The second pathway involved the direct substitution of the NO_2 group by OH *via* a phenol radical intermediate to form catechol (RT = 21.91 min). Catechol was then oxidized to *o*-benzoquinone (RT = 16.77 min) and underwent ring opening to produce *cis–cis*-muconic acid (RT = 20.57 min). The successive oxidative cleavage of muconic acid by $^{\bullet}OH$ radicals resulted in the formation of maleic acid (RT = 12.87 min), followed by oxalic acid (RT = 4.57 min) and formic acid (RT = 7.44 min), which were eventually degraded into carbon dioxide and water. Fig. 10 illustrates the possible Fenton-like degradation pathway of 2-NP on the Fe_3O_4/MIL-88A/BC composite.

3.6. Stability of the Fe_3O_4/MIL-88A/BC catalyst

To confirm the stability of Fe_3O_4/MIL-88A/BC, it was crucial to examine the metal leaching after the Fenton-like reaction and study the recyclability of the catalyst.

3.6.1. Recyclability study. A cycling test was executed for five cycles of Fenton-like degradation of 2-NP to investigate the recyclability of the Fe_3O_4/MIL-88A/BC catalyst (Fig. 11A). Surprisingly, the results observed the superb recyclability of Fe_3O_4/MIL-88A/BC, where its activity decreased by 8.54% after

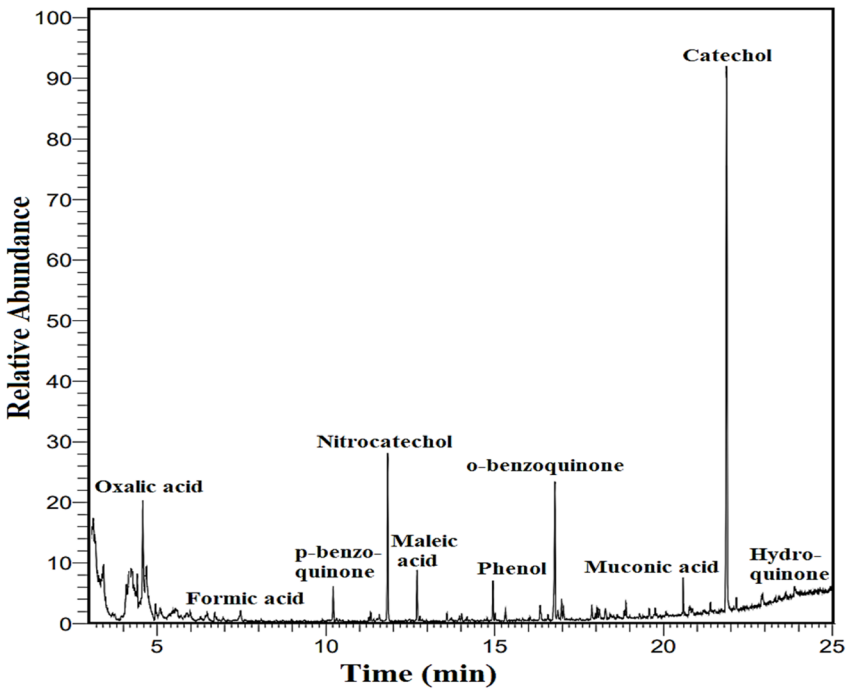

Fig. 9 GC-MS of 2-NP after Fenton-like degradation by the Fe_3O_4/MIL-88A/BC composite.

Open Access Article. Published on 13 June 2025. Downloaded on 3/31/2026 11:27:39 AM.
This article is licensed under a Creative Commons Attribution-NonCommercial 3.0 Unported Licence.

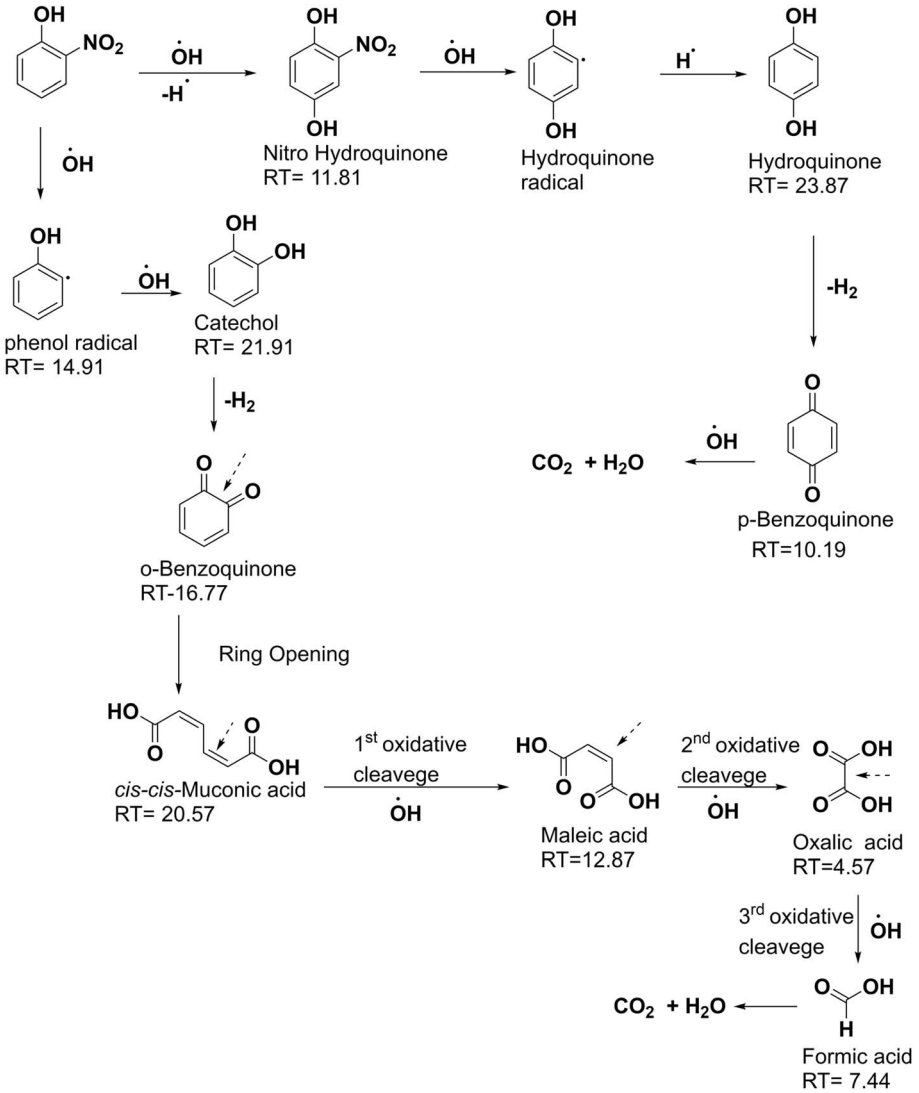

Fig. 10 Schematic representation of the degradation of 2-NP by the Fe_3O_4/MIL-88A/BC composite.

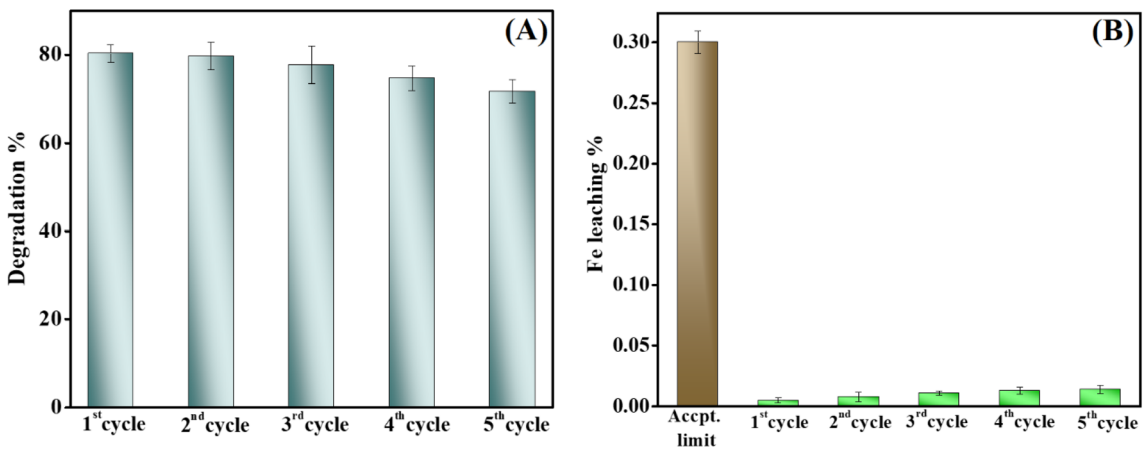

Fig. 11 (A) Cycling test of the Fe_3O_4/MIL-88A/BC catalyst for five 2-NP degradation cycles and (B) leaching test of Fe species from the Fe_3O_4/MIL-88A/BC composite during the five degradation cycles.

© 2025 The Author(s). Published by the Royal Society of Chemistry

Open Access Article. Published on 13 June 2025. Downloaded on 3/31/2026 11:27:39 AM. This article is licensed under a Creative Commons Attribution-NonCommercial 3.0 Unported Licence.

the 5th cycle. This propitious recyclability owes to the catalyst; the magnetic character of Fe_3O_4/MIL-88A/BC provides perfect and fast separation using a magnet without weight loss. Meanwhile, the decline in the catalytic activity after the o-NP degradation cycles may be explained by the possible adsorption interactions between o-NP and Fe_3O_4/MIL-88A/BC, which resulted in incomplete recovery of the catalyst, since some o-NP molecules were still attached to the active groups of the catalyst. In addition, the regeneration of Fe^{2+} could not occur completely because not all Fe^{3+} species were reduced to Fe^{2+}. Furthermore, the expected Fe leaching from Fe_3O_4/MIL-88A/BC after the sequential Fenton-like degradation of o-NP could impact the efficacy of the catalyst.

3.6.2. Metal leaching. XPS surveys of authentic and used Fe_3O_4/MIL-88A/BC catalysts revealed an increment in the carbon content from 49.56% to 61.85% and a diminution in oxygen percentage from 41.88% to 27.73%, which may be attributed to the conversion of some oxygen-centered EPFRs to carbon-centered EPFRs after the catalytic degradation reaction of 2-NP.[17] The appearance of a tiny peak belonging to N1s (1.98%) is attributed to the present nitro group in 2-NP. Interestingly, the Fe leaching percentage from Fe_3O_4/MIL-88A/BC after the Fenton-like degradation of 2-NP was approximately 1.97%, confirming the viability of the chemical structure of the as-fabricated catalyst. For a further indication of the chemical stability of Fe_3O_4/MIL-88A/BC, the Fe leaching percentage was evaluated by ICP-OES, as shown in Fig. 11B. The Fe leaching percentage from the Fe_3O_4/MIL-88A/BC catalyst after Fenton-like degradation of 2-NP was 0.005, 0.008, 0.011, 0.0013, and 0.014 mg L^{-1}. The acceptable limit of Fe ions in drinking water is 0.3 mg L^{-1} according to the USEPA. This finding not only confirms the chemical composition stability of Fe_3O_4/MIL-88A/BC but also indicates the eco-friendliness of the catalyst.

4. Conclusion

Fe_3O_4/MIL-88A/BC was successfully fabricated, and its physical and chemical characteristics were identified by various characterization analyses, including SEM, ZP, XRD, XPS, and FTIR. The SEM image revealed the diamond-shaped MIL-88A fabricated using the solvothermal approach. The FTIR and XRD patterns of Fe_3O_4/MIL-88A/BC demonstrated a good combination of Fe_3O_4, MIL-88A, and BC inside the composite structure. The results of the laboratory experiments showed that the DE of 2-NP by the H_2O_2/Fe_3O_4/MIL-88A/BC catalytic system reached 91.04% at pH = 5, H_2O_2 concentration = 500 mg L^{-1}, Fe_3O_4/MIL-88A/BC = 10 mg, and 120 min. The quenching test deduced 2-NP degradation *via* the radical pathway, with $^{\bullet}OH$ as the main reactive O-species. The XPS analysis of pristine and used Fe_3O_4/MIL-88A/BC suggested the occurrence of the Fenton-like degradation of 2-NP by the Haber–Weiss mechanism and EPFRs-based BC. Notably, the ability of BC to donate electrons enabled it to be the controller in the half of the redox cycle ($Fe^{3+} \rightarrow Fe^{2+}$) and the continuity of the Fenton-like degradation of 2-NP.

Based on our in-depth study, we recommend our catalyst as a superb catalyst for Fenton-like reactions, taking into consideration increasing the number of transition metals in the catalyst to expand the redox cycle by doping metal species, fabricating bimetallic/binary MOF, or adding layered double/triple hydroxide to the catalyst matrix. These transition metals boost the concentration of the generated $^{\bullet}OH$ radicals and work together with BC to recover the Fe^{2+} ions, thereby further improving the degradation efficacy and catalyst recyclability. Furthermore, the Fenton/Fenton-like degradation of 2-NP requires further investigation because there is a shortage of published research highlighting this topic. Excessive studies are essential to propose other degradation pathways for 2-NP and to examine the toxicity of the produced intermediates.

Data availability

The data that support the findings of this study are available from the corresponding author upon reasonable request.

Conflicts of interest

There are no conflicts to declare.

Funding

This work was supported by the Deanship of Scientific Research, Vice Presidency for Graduate Studies and Scientific Research, King Faisal University, Saudi Arabia (Project No. KFU252061).

Acknowledgements

JA and MSA acknowledge "the Deanship of Scientific Research, Vice Presidency for Graduate Studies and Scientific Research, King Faisal University, Saudi Arabia, for financial support under the annual funding track [KFU252061].

References

1 B. S. Marques, K. Dalmagro, K. S. Moreira, M. L. Oliveira, S. L. Jahn, T. A. de Lima Burgo and G. L. Dotto, *J. Alloys Compd.*, 2020, **838**, 155628.
2 A. M. Omer, A. S. Eltaweil, A. M. Abdelhamed, E. M. Abd El-Monaem and G. M. El-Subruiti, *Sci. Rep.*, 2024, **14**, 14463.
3 D. Ewis, M. M. Ba-Abbad, A. Benamor, N. Mahmud, M. Nasser, M. El-Naas and A. W. Mohammad, *Int. J. Environ. Res.*, 2022, **16**, 23.
4 D. Khan, J. Kuntail and I. Sinha, *J. Mol. Graphics Modell.*, 2022, **116**, 108251.
5 Y. Yang, Y. Gu, H. Lin, B. Jie, Z. Zheng and X. Zhang, *J. Colloid Interface Sci.*, 2022, **608**, 2884–2895.
6 A. S. Eltaweil, A. M. Galal, E. M. Abd El-Monaem, N. Al Harby and M. El Batouti, *Nanomaterials*, 2024, 14.
7 J. Lu, M. Yue, W. Cui, C. Sun and L. Liu, *Colloids Surf., A*, 2022, **655**, 130222.
8 Y. Liu and J. Wang, *Chem. Eng. J.*, 2023, **466**, 143147.
9 E. M. Abd El-Monaem, A. M. Omer and A. S. Eltaweil, *J. Polym. Environ.*, 2024, **32**, 2075–2090.

Open Access Article. Published on 13 June 2025. Downloaded on 3/31/2026 11:27:39 AM. This article is licensed under a Creative Commons Attribution-NonCommercial 3.0 Unported Licence.

10 J. Tang and J. Wang, *Environ. Sci. Technol.*, 2018, **52**, 5367–5377.
11 V. P. Viswanathan, S. V. Mathew, D. P. Dubal, N. N. Adarsh and S. Mathew, *ChemistrySelect*, 2020, **5**, 7534–7542.
12 H. Fu, X.-X. Song, L. Wu, C. Zhao, P. Wang and C.-C. Wang, *Mater. Res. Bull.*, 2020, **125**, 110806.
13 S. M. Shaheen, N. K. Niazi, N. E. Hassan, I. Bibi, H. Wang, D. C. Tsang, Y. S. Ok, N. Bolan and J. Rinklebe, *Int. Mater. Rev.*, 2019, **64**, 216–247.
14 J. Wang and S. Wang, *J. Cleaner Prod.*, 2019, **227**, 1002–1022.
15 E. M. Abd El-Monaem, A. M. Omer, G. M. El-Subruiti, M. S. Mohy-Eldin and A. S. Eltaweil, *Biomass Convers. Biorefin.*, 2024, **14**, 1697–1709.
16 R. Deng, H. Luo, D. Huang and C. Zhang, *Chemosphere*, 2020, **255**, 126975.
17 X. Ruan, Y. Sun, W. Du, Y. Tang, Q. Liu, Z. Zhang, W. Doherty, R. L. Frost, G. Qian and D. C. Tsang, *Bioresour. Technol.*, 2019, **281**, 457–468.
18 M. Jin, M. Long, H. Su, Y. Pan, Q. Zhang, J. Wang, B. Zhou and Y. Zhang, *Environ. Sci. Pollut. Res.*, 2017, **24**, 1926–1937.
19 R. C. Costa, F. C. Moura, J. Ardisson, J. Fabris and R. Lago, *Appl. Catal., B*, 2008, **83**, 131–139.
20 G. Fang, J. Gao, C. Liu, D. D. Dionysiou, Y. Wang and D. Zhou, *Environ. Sci. Technol.*, 2014, **48**, 1902–1910.
21 Y. Pan, M. Zhou, X. Li, L. Xu, Z. Tang and M. Liu, *Sep. Purif. Technol.*, 2016, **169**, 83–92.
22 L. Yu, X. Yang, Y. Ye and D. Wang, *RSC Adv.*, 2015, **5**, 46059–46066.
23 L. Xu and J. Wang, *Environ. Sci. Technol.*, 2012, **46**, 10145–10153.
24 G. Fang, C. Zhu, D. D. Dionysiou, J. Gao and D. Zhou, *Bioresour. Technol.*, 2015, **176**, 210–217.
25 G. Ren, K. Zhao and L. Zhao, *RSC Adv.*, 2020, **10**, 39973–39980.
26 E. M. Abd El-Monaem, N. Al Harby, M. E. Batouti and A. S. Eltaweil, *Nanomaterials*, 2023, **14**, 54.
27 X. Liao, F. Wang, F. Wang, Y. Cai, Y. Yao, B.-T. Teng, Q. Hao and L. Shuxiang, *Appl. Catal., B*, 2019, **259**, 118064.
28 F. Sang, Z. Yin, W. Wang, E. Almatrafi, Y. Wang, B. Zhao, J. Gong, C. Zhou, C. Zhang and G. Zeng, *J. Cleaner Prod.*, 2022, **378**, 134459.
29 J.-H. Park, J. J. Wang, R. Xiao, N. Tafti, R. D. DeLaune and D.-C. Seo, *Bioresour. Technol.*, 2018, **249**, 368–376.
30 S. Zhao, Y. Li, M. Wang, B. Chen, Y. Zhang, Y. Sun, K. Chen, Q. Du, Z. Jing and Y. Jin, *Microporous Mesoporous Mater.*, 2022, **345**, 112241.
31 A. M. Omer, M. El-Sayed, E. M. Abd El-Monaem, G. M. El-Subruiti and A. S. Eltaweil, *Int. J. Biol. Macromol.*, 2023, **253**, 127437.
32 A. S. Eltaweil, S. S. Bakr, E. M. Abd El-Monaem and G. M. El-Subruiti, *Environ. Sci. Pollut. Res.*, 2023, **30**, 75332–75348.
33 E. M. Abd El-Monaem, M. Hosny and A. S. Eltaweil, *Chem. Eng. Sci.*, 2024, **287**, 119707.
34 B. S. Marques, K. Dalmagro, K. S. Moreira, M. L. Oliveira, S. L. Jahn, T. A. De Lima Burgo and G. L. Dotto, 2020.
35 H. Ma, Z. Xu, W. Wang, X. Gao and H. Ma, *RSC Adv.*, 2019, **9**, 39282–39293.
36 J. Chen, X. Sun, L. Lin, X. Dong and Y. He, *Chin. J. Chem. Eng.*, 2017, **25**, 775–781.
37 A. Jawad, J. Lang, Z. Liao, A. Khan, J. Ifthikar, Z. Lv, S. Long, Z. Chen and Z. Chen, *Chem. Eng. J.*, 2018, **335**, 548–559.
38 X. Li, K. Cui, Z. Guo, T. Yang, Y. Cao, Y. Xiang, H. Chen and M. Xi, *Chem. Eng. J.*, 2020, **379**, 122324.
39 A. S. Eltaweil, N. Al Harby, A. I. Osman, M. Alrasheedi, Y. Su and E. M. Abd El-Monaem, *J. Ind. Eng. Chem.*, 2025, **143**, 704–716.
40 N. A. Youssef, S. A. Shaban, F. A. Ibrahim and A. S. Mahmoud, *Egypt. J. Pet.*, 2016, **25**, 317–321.
41 T. Geng, J. Yan, B. Li, H. Yan, L. Guo, Q. Sun, Z. Guan, C. Zhao, J. Xu and W. Wang, *Results Chem.*, 2024, **11**, 101795.
42 J. Singh, J. Yang, Y. Chang and J. Koduru, *Chem. Eng. J.*, 2017, **307**, 74–84.
43 G. Rózsa, M. Náfrádi, T. Alapi, K. Schrantz, L. Szabó, L. Wojnárovits, E. Takács and A. Tungler, *Appl. Catal., B*, 2019, **250**, 429–439.
44 Y. Wu, X. Li, H. Zhao, F. Yao, J. Cao, Z. Chen, F. Ma, D. Wang and Q. Yang, *Chemosphere*, 2022, **287**, 132061.
45 X. Li, H. Zhou, R. Qian, X. Zhang and L. Yu, *Chin. Chem. Lett.*, 2025, **36**, 110036.

© 2025 The Author(s). Published by the Royal Society of Chemistry